Nuclear Engineering and Design 54 (1979) 49–66


# NUMERICAL INVESTIGATION OF RADIAL MIXING CAPABILITIES IN STRONGLY BUOYANCY-INFLUENCED VERTICAL, TURBULENT CHANNEL FLOWS

G. GRÖTZBACH

*Institut für Reaktorentwicklung, Kernforschungszentrum Karlsruhe GmbH, Postfach 3640, D–7500 Karlsruhe, Fed. Rep. Germany*

Received 2 April 1979

The flow behavior in the HDR downcomer during setting of the initial conditions for blowdown tests is investigated with the numerical simulation program for turbulent channel flows, TURBIT–3. This computer code is based on the complete 3-dimensional non-stationary basic equations for mass, momentum and heat. The subgrid scale models used for the turbulence structures not directly resolved by the grid are extended to take into account the buoyancy in the case of turbulent channel flow. The extended computer code is used to investigate how fast differences in temperature can be reduced, which are caused by inadequate mixing in the lower plenum during upward flow in the downcomer under conditions of mixed convection. It appears that, contrary to the computations neglecting the influences of buoyancy, the temperature differences are rapidly reduced already in the entrance zone of the downcomer. In this zone, local recirculation takes place in the cold region, which is quickly suppressed with increasing distance from the entrance by the intensification of the turbulence effects. A hot chimney extending through the whole downcomer cannot develop. Already at half level, the influence of buoyancy can be considered to be negligible in the downcomer which is assumed adiabatic. Under these conditions it should be possible in principle to set the enthalpy stratification by the planned layout of the experiment in the HDR-pressure vessel.

## 1. Introduction

In the HDR-safety research program, blowdown tests are carried out inter alia at the shut down superheating steam reactor (Heissdampfreaktor HDR) in Kahl [1]. These tests serve the purpose of investigating the fluid and structure dynamical load of the reactor pressure vessel and its internals in the case of sudden depressurization by rupture of a cold water feeding pipe. It is intended to start these tests from a temperature field within the pressure vessel, which is typical of the operating condition of a pressurized water reactor. This means that within the core barrel, higher temperatures, rising towards the top, are to be set as compared with the downcomer between the core barrel and the pressure vessel wall (fig. 1). This enthalpy stratification is to be achieved by supply of hot water (h) in the upper plenum and by supply of colder water (c) in the lower plenum. The mixed water (m) is withdrawn at the upper end of the downcomer.

The radial temperature gradient within and at the core barrel developing in this flow gives rise to some problems which are connected with the superposition of natural convection with forced flow phenomena within the core barrel and in the downcomer. The possible disturbances within the core barrel are of minor importance because of the predominantly stable stratification, the more so since they do not counteract the objective of flow guidance, i.e. to set a temperature field decreasing from top to bottom. By contrast, considerable uncertainties occur in the downcomer. Above all, the questions are raised whether

(1) the generation of a "chimney" might be promoted by the radial heat flow through the core barrel in the downcomer (hot, accelerating zone on a reducing cross section near the core barrel and cold, decelerating zone on an expanding cross section on the pressure vessel wall side);

(2) by azimuthal arrangement of the nozzles a "chimney" as mentioned under (1) might be generated in the azimuthal direction over rather large regions in

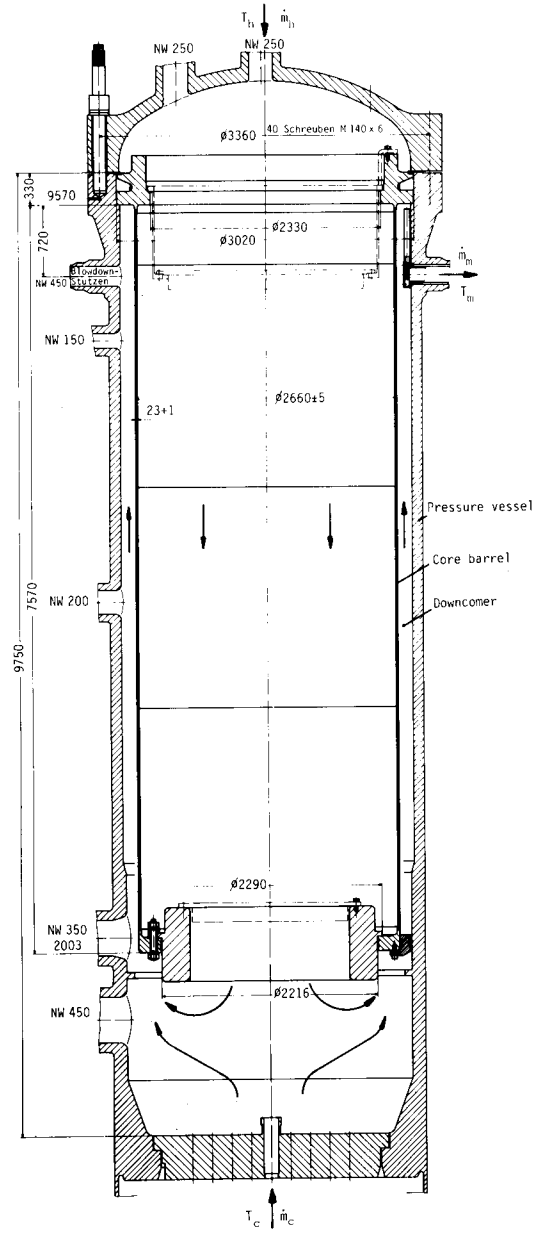


Fig. 1. Flow guidance in the HDR pressure vessel for setting enthalpy stratification.

the downcomer;

(3) by inadequate mixing of the two mass flows, generation of a chimney is supported equally in the downcomer;

(4) or whether by intensified turbulent mixing of the two mass flows in the downcomer a radially almost constant temperature profile is established which will not result in influences by natural convection.

These problems were investigated prior to the experiments with an extended version of the TURBIT–2 numerical simulation program [2]. The method of direct numerical simulation of turbulent flows is based on the complete time-dependent, three-dimensional equations for mass, momentum and heat. Using finite difference grids with finite spatial resolution, subgrid scale models are required for consideration of the momentum and heat transport within the grid cells. Turbulence elements greater than a few grid cells are simulated directly. Therefore, all those quantities of turbulence may be calculated from the numerical results, which are largely dominated by gross-scale turbulence.

For turbulent channel flows, this method was used for the first time by Deardorff [3]. The method was extended by Schumann [4] for application to non-equidistant meshes, to finite Reynolds numbers and to a more realistic consideration of the subgrid scale fluxes in the near wall region. Further extensions by Grötzbach [2] relate to the applicability to low Reynolds number flows, coarse grids, rough walls and additional simulation of the temperature field. Thus, the accuracy of the numerical results becomes comparable to experimental data, even if rather coarse grids are used and short time intervals are calculated [2,5].

Because of these advantages, the method of direct numerical simulation provides a good possibility for studying the problems of the strongly buoyancy-influenced convection as characterized above. It is the purpose of this publication to report about the essential results of the numerical investigation of the problems indicated. Initially, the features of the numerical technique used will be explained together with the related subgrid scale model.

## 2. Basic equations of the simulation method

### *2.1. Normalized basic equations*

The basic equations for mixed convection are the continuity equation (mass balance), the temperature equation (enthalpy balance), and the Navier–Stokes equation extended by the buoyancy terms (vectorial momentum balance). For simplification, the validity

of the Boussinesq approximation is assumed, i.e. the assumption is made that the material properties can be considered as constant in all terms of these equations, except for the buoyancy term $\hat{g}_i\hat{\beta}(\hat{T}_{\mathrm{ref}} - \hat{T})$ (variables marked by ˆ possess dimensions).

$$\frac{\partial u_i}{\partial x_i} = 0 \tag{1a}$$

$$\frac{\partial u_i}{\partial t} + \frac{\partial}{\partial x_j}(u_i u_j) = -\frac{\partial p}{\partial x_i} - \left\langle \frac{\partial p}{\partial x_i} \right\rangle + \frac{\mathrm{Gr}_{0i}}{\mathrm{Re}_0^2}(T_{\mathrm{ref}} - T)$$

$$+ \frac{1}{\mathrm{Re}_0}\frac{\partial}{\partial x_j}\left(\frac{\partial u_i}{\partial x_j} + \frac{\partial u_j}{\partial x_i}\right), \quad \text{for } i = 1, 2, 3 \tag{1b}$$

$$\frac{\partial T}{\partial t} + \frac{\partial}{\partial x_j}(T u_j) = \frac{1}{\mathrm{Re}_0 \mathrm{Pr}}\frac{\partial}{\partial x_j}\frac{\partial T}{\partial x_j}. \tag{1c}$$

As below, the Einstein summation rule must be applied here to all terms bearing the same subscripts twice. The pressure term has been split in a purely formal way into a term averaged over time ($\langle y \rangle$ means the time average value of $y$) and a time dependent one, the merely turbulent contribution of variation. The dimensionless numbers appearing in eqs. (1) are defined as follows by the normalizing variables bearing the subscript 0: Reynolds number

$$\mathrm{Re}_0 = \hat{u}_0 \hat{D}/\hat{\nu}, \tag{2a}$$

Prandtl number

$$\mathrm{Pr} = \hat{\nu}/\hat{a}, \tag{2b}$$

Grashof number

$$\mathrm{Gr}_{0i} = \hat{g}_i \hat{\beta} \hat{T}_0 \hat{D}^3/\hat{\nu}^2. \tag{2c}$$

All lengths are normalized with the channel width $\hat{D}$. The time scale introduced was $\hat{t}_0 = \hat{D}/\hat{u}_0$ ($D$ = channel width) and the pressure scale $\hat{p}_0 = \hat{\rho}_0 \hat{u}_0^2$. The free normalizing variables are defined as far as possible consistently with those applicable to TURBIT–2, mainly because the formulae for the wall conditions are taken over for the velocity field. Consequently, the wall shear stress velocity $\hat{u}_\tau$ averaged over both walls is equally chosen for $\hat{u}_0$

$$\hat{u}_0 = \hat{u}_\tau = \sqrt{\hat{\tau}_w/\hat{\rho}}, \tag{3}$$

offering the advantage that the imposed pressure gradient in the main flow direction $x_1$ (fig. 2) can be calculated from a force balance of the flow volume to be $\langle \partial p/\partial x_1 \rangle \equiv 2$.

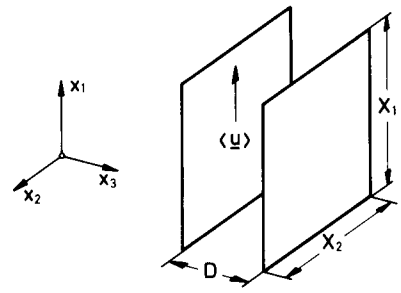


Fig. 2. Orientation of the coordinate system and periodical boundary conditions at the channel recorded.

Considering the case studied here of a channel adiabatic on both sides the temperature difference between the two walls at the time $t = 0$ is introduced as a normalizing temperature:

$$\hat{T}_0 = (\hat{T}_{w1} - \hat{T}_{w2})|_{t=0}. \tag{4}$$

The reference temperature $T_{\mathrm{ref}}$ in the buoyancy term is set equal to the volume averaged value ${}^{v}\langle T \rangle$ of the temperature in the entire channel in order to avoid a net contribution of the buoyancy term to the pressure gradient imposed.

The dimensionless numbers to be predetermined as by eqs. (2) have been correlated as follows to those usually employed:

$$\mathrm{Re}_0 = \mathrm{Re}_\tau = \mathrm{Re}/{}^{v}\langle u_1 \rangle, \quad \mathrm{Re} = {}^{v}\langle u_1 \rangle \hat{D}/\hat{\nu}, \tag{5a}$$

$$\mathrm{Gr}_{0i} = \mathrm{Gr}_i, \quad \mathrm{Gr}_i = \hat{g}_i \hat{\beta}(\hat{T}_{w1} - \hat{T}_{w2}) \hat{D}^3/\hat{\nu}^2. \tag{5b}$$

The volume averaged value of the mean velocity ${}^{v}\langle u_1 \rangle$ can be calculated from eq. (5a) for a given friction factor $C_f$ to be

$$\mathrm{Re}_\tau = \mathrm{Re}\sqrt{C_f/8}. \tag{6}$$

Herewith, the necessary normalizations of the basic equations have been introduced for use of TURBIT–3.

### 2.2. *Volume averaged conservation equations*

The method of direct numerical simulation presented in this paper is based on a finite difference scheme which solves the complete Navier–Stokes equation, the continuity and the thermal energy equations. Following Schumann [4] for the derivation of

this scheme, the basic equations (1) are averaged over finite grid volumes $V = \Delta x_1\,\Delta x_2\,\Delta x_3$:

$$ {}^{v}\overline{y} = \frac{1}{\Delta x_1\,\Delta x_2\,\Delta x_3} \times \int_{\Delta x_1}\int_{\Delta x_2}\int_{\Delta x_3} y(x_1', x_2', x_3')\,\mathrm{d}x_3'\,\mathrm{d}x_2'\,\mathrm{d}x_1' , \tag{7a} $$

$$ {}^{v}\overline{\frac{\partial y}{\partial x_1}} = \frac{1}{\Delta x_1}\left[{}^{1}\overline{y}(x_1 + \tfrac{1}{2}\Delta x_1) - {}^{1}\overline{y}(x_1 - \tfrac{1}{2}\Delta x_1)\right] = \delta_1\,{}^{1}\overline{y} . \tag{7b} $$

Hereby, the triple integral defining the average ${}^{v}\overline{y}$, eq. (7a) is integrated by parts with respect to the divergence type terms, eq. (7b) so that the average is expressed in terms of finite differences of surface mean values ${}^{i}\overline{y}$. This allows the use of grid cells with different spacings $\Delta x_i$. The resultant equations are the averaged mass or continuity equation, the averaged momentum or Navier–Stokes equation, and the averaged thermal energy equation:

$$ \delta_i\,{}^{i}\overline{u}_i = 0 , \tag{8a} $$

$$ \frac{\partial}{\partial t}{}^{v}\overline{u}_i = -\delta_j\,{}^{j}\overline{u}_i\,{}^{j}\overline{u}_j - \delta_j\,{}^{j}\overline{u_i'u_j'} + \delta_j\left(\frac{1}{\mathrm{Re}_0}\frac{{}^{j}\partial\overline{u_i}}{\partial x_j}\right) - \delta_i\,{}^{i}\overline{p} - \delta_i\langle{}^{i}\overline{p}\rangle + \frac{\mathrm{Gr}_{0i}}{\mathrm{Re}_0^2}({}^{v}\langle T\rangle - {}^{v}\overline{T}) , \tag{8b} $$

$$ \frac{\partial}{\partial t}{}^{v}\overline{T} = -\delta_j\,{}^{j}\overline{u}_j\,{}^{j}\overline{T} - \delta_j\,{}^{j}\overline{u_j'T'} + \delta_j\left(\frac{1}{\mathrm{Re}_0\mathrm{Pr}}\frac{{}^{j}\partial\overline{T}}{\partial x_j}\right). \tag{8c} $$

With a few exceptions, almost all terms of the equation system were directly brought into a finite difference form by partial integration. The rest of partial derivations are substituted by linear finite difference approximations.

### 2.3. Subgrid scale flux approximations

No considerable approximations have been involved so far. However, the volume averaged equations (8) are yet unclosed. For the unknown subgrid scale (SGS) fluxes of momentum ${}^{ij}\overline{u_i'u_j'}$ and heat ${}^{j}\overline{u_j'T'}$, special subgrid scale models are introduced which reflect the momentum and heat transport caused by the vortices not subjected to spatial resolution in the grid. These models have been tested and used in channel flows with differing molecular Prandtl numbers, smooth and roughened walls, and with secondary flows [2,5]. In principle, they largely rely on statistical turbulence models. However, their influence is heavily reduced by the choice of the mesh width as a characteristic length scale. The events taking place within the subgrid scale structure largely obey universal laws which can be derived from the theory of isotropic turbulence.

To be able to employ this theory strictly to the theoretical determination of the model constants, the models were split formally into a time dependent part which can be treated by the theory of isotropic turbulence and a time or ensemble averaged part, respectively, which takes into account the inhomogeneities caused by the walls. For both parts gradient diffusion is assumed, analogous to molecular diffusion:

$$ {}^{ij}\overline{u_i'u_j'} = -{}^{ij}\mu(D_{ij} - \langle D_{ij}\rangle) - {}^{ij}\mu^{*}\langle D_{ij}\rangle , \tag{9a} $$

$$ {}^{j}\overline{u_j'T'} = -{}^{j}a_t\delta_j({}^{j}\overline{T} - \langle{}^{j}\overline{T}\rangle) - {}^{j}a_t^{*}\delta_j\langle{}^{j}\overline{T}\rangle , \tag{9b} $$

where $D_{ij} = \partial u_i/\partial x_j + \partial u_j/\partial x_i$. The unknown subgrid scale eddy diffusivities ${}^{ij}\mu$ and ${}^{ij}\mu^{*}$, and eddy conductivities ${}^{j}a_t$ and ${}^{j}a_t^{*}$ are calculated from modified common turbulence models:

According to Schumann [4], the *isotropic* eddy diffusivities ${}^{ij}\mu$ are determined by a Prandtl energy length scale type model. The other parts of the models are as in [2]. The isotropic eddy conductivities ${}^{j}a_t$ are modeled in an analogous manner, assuming that the subgrid scale heat flux depends on the velocity fluctuations within the grid cells:

$$ {}^{ij}\mu = C_2\,{}^{ij}C({}^{j}F\,{}^{j}C_5\,{}^{v}\overline{E'})^{1/2} , \tag{10a} $$

$$ {}^{j}a_t = C_{T2}\,{}^{j}C_T({}^{j}F\,{}^{j}C_5\,{}^{v}\overline{E'})^{1/2} . \tag{10b} $$

Here, the characteristic length scale is the surface area ${}^{j}F = \Delta x_1\,\Delta x_2\,\Delta x_3/\Delta x_j$ of the grid cell over which the averaged eqs. (9a) and (9b), are defined, and the characteristic energy is the SGS-kinetic energy ${}^{v}\overline{E'}$ of the unresolved velocity fluctuations, for which we have to integrate an additional transport equation.

The coefficients ${}^{j}C_5$, ${}^{ij}C$ and ${}^{j}C_T$ account for geometrical details of the mesh and the finite difference scheme and are of order one. Because of the formal splitting eq. (9) of the SGS-fluxes, these coefficients and the dominating coefficients, $C_2$ and $C_{T2}$ may be determined theoretically, assuming locally isotropic subgrid scale turbulence. For this purpose, we assume the validity of the well-known Kolmogorov spectra

for kinetic energy and temperature variances (for details see Grötzbach [2]). The natural convection mainly acting on the large scale structures, see for example Turner [6], can be left out of consideration when calculating the subgrid scale constants, since the subgrid scale constants respond at a relatively moderate degree to changes of the energy spectra within the range of large vortices.

The *inhomogeneous* eddy diffusivities ${}^{ij}\mu^*$ and eddy conductivities ${}^{j}a_t^*$ are derived from modified common mixing length models:

$$ {}^{ij}\mu^* = \delta_{1i}\delta_{3j} l^2 \left| \left\langle \frac{{}^{\upsilon}\overline{\partial u_i}}{\partial x_3} \right\rangle \right| f(C_{10}, \Delta x_i) , \tag{11a} $$

$$ {}^{j}a_t^* = \delta_{3j} l l_T \left| \left\langle \frac{{}^{\upsilon}\overline{\partial T}}{\partial x_3} \right\rangle \right| f_T(C_{T10}, \Delta x_i) . \tag{11b} $$

The mixing lengths $l$ and $l_T$ are well-known functions of the distance from the wall and the wall roughness. In addition, $l_T$ depends on the molecular Prandtl number of the fluid. We use a Nikuradse–Van Driest and Cebeci formulation, respectively. The crucial factors in eq. (11) are the damping functions $f$ and $f_T$ formed by those mesh surfaces ${}^{j}F$ over which also the contributing velocity and temperature fluctuations have been averaged:

$$ f(C_{10}, \Delta x_i) = \mathrm{Min}\{l, C_{10}({}^{1}F\ {}^{3}F)^{1/4} F_0^{-1/2}\} , \tag{12a} $$

$$ f_T(C_{T10}, \Delta x_i) = \mathrm{Min}\{l, (C_{10}\, C_{T10})^{1/2}({}^{3}F\ {}^{2}\Delta x_3)^{1/5} F_{T0}^{-1/2}\} . \tag{12b} $$

They are designed so that for very coarse meshes the SGS models become equal to the common models for time averaged turbulence ($f, f_T \equiv 1$). For very fine resolution the functions vanish ($f, f_T \to 0$) since in this case all SGS fluxes are described by the isotropic parts. The normalization surfaces $F_0 = F_{T0} = 1.28$ were derived from experimental results for the two point-correlations of the velocity fluctuations. Using these values, the constants $C_{10} = 2$ and $C_{T10} = 1$ are ultimately adapted in a numerical -empirical mode within the frame of a sensitivity study [2].

It was found in this sensitivity study that within the range of ultimately used values of all constants the numerical results respond but moderately to changes of the constants. The reason why the subgrid scale models used here exhibit less dependencies on the subgrid scale coefficients than is usually the case, e.g., also with respect to the models used by Deardorff [3], must be attributed to the subgrid scale structure energy equation used in addition which causes non-linear coupling between the large scale structure and the subgrid structure represented by the models [2, Appendix 5].

From Turner [6] and Wippermann [7], it is known for meteorological flows that both the turbulent exchange coefficients and the mixing lengths themselves depend on the influence of natural convection. From experience gathered by Khosla et al. [8], this applies equally to vertical pipe flows. Unfortunately, the existing models, e.g., by Wassel and Catton [9], are valid only for horizontal flows along plane plates, and by Seban and Behnia [10] for round, buoyant jets in a quiescent surrounding only. This implies that an influence of buoyancy on the inhomogeneous parts of the subgrid scale model cannot be formulated so as to be meaningful. According to the results of the sensitivity study mentioned above, the effects of this lack can be considered minor in direct numerical simulation, contrary to the statistical turbulence models since, on the one hand, the subgrid scale models generally describe only the turbulence portion not resolved by the grid and, on the other hand, the isotropic parts of the models completely take into account the influence of buoyancy. The respective extension of the model will be demonstrated below.

### 2.4. Additional SGS energy equation

The characteristic energy used in the isotropic parts, eq. (10) of the SGS flux models is the subgrid scale kinetic energy ${}^{\upsilon}\overline{E'} = \frac{1}{2}\overline{{}^{\upsilon}(u_i - {}^{\upsilon}\overline{u_i})^2}$. It is calculated using an additional time dependent three-dimensional transport equation as in principal deduced by Schumann [4] and improved by Grötzbach [2]:

$$ \frac{\partial {}^{\upsilon}\overline{E'}}{\partial t} = \text{production} + \text{diffusion} - \text{convection} - \text{dissipation} . \tag{13} $$

The subgrid scale structure shear stresses ${}^{j}\overline{u_i' u_j'}$ contained in the production term

$$ \text{production} = -\,{}^{j}\overline{u_i' u_j'}\, \delta_j {}^{j}\overline{u_i} \tag{14} $$

are represented by the complete subgrid scale model eqs. (9a), (10a) and (11a). In case this energy equation is to be applied to mixed convection or pure natural convection according to Deardorff [11], an additional production term must be introduced here which describes the subgrid scale turbulence production by variation of the density. Considering normalization according to section 2.1, one obtains as a substitute of eq. (14) for the production term:

$$\text{production} = -\overline{{}^{j}u_i'u_j'}\,\delta_j\,\overline{{}^{j}u_i} - \frac{\mathrm{Gr}_{0j}}{\mathrm{Re}_0^2}\overline{{}^{j}u_j'T'}\,. \tag{15}$$

The turbulent subgrid scale heat flux $\overline{{}^{j}u_j'T'}$ obtained in the additional term can be described by the complete temperature subgrid scale model eqs. (9b), (10b) and (11b).

The extended model for SGS dissipation $\overline{{}^{v}\epsilon}$, like the production term accounts for inhomogeneity effects. In addition, it allows application of the method to smaller Reynolds numbers ($\mathrm{Re} \gtrsim 10^4$) and coarser grids. We use the Rotta-type formulation:

$$\overline{{}^{v}\epsilon} = C_3\,\overline{{}^{v}E}^{3/2}/\mathrm{Min}(h, C_{31}l) + C_{32}\nu\,\overline{{}^{v}E'}/\mathrm{Min}(h, C_{31}l)^2\,. \tag{16}$$

The first term is dominant at large Reynolds numbers, while the second term dominates at small Reynolds numbers. The minimum function gives the grid size $h = (\Delta x_1\,\Delta x_2\,\Delta x_3)^{1/3}$ as a characteristic length scale in the core of the flow, and the mixing length $l$ in the near wall region. For the determination of the coefficient $C_3$ and of the constants $C_{31} = 0.74$ and $C_{32} = 20.0$, the Laser–Doppler measurements by Lörcher [12] for a plane channel have been used.

Due to lack of validated information, it is supposed that the dissipation in the subgrid scale structure is equally free from phenomena of natural convection as the convection and diffusion terms which had been taken over from Schumann [4].

### *2.5. Influence of natural convection on the wall conditions*

In the basic equations (8), the following terms appear at the walls

$$-\frac{1}{\mathrm{Re}_0}\left.\frac{\partial\overline{{}^{3}u_1}}{\partial x_3}\right|_{\mathrm{w}} = \tau_{\mathrm{w}}\,, \tag{17a}$$

$$-\frac{1}{\mathrm{Re}_0\mathrm{Pr}}\left.\frac{\partial\overline{{}^{3}T}}{\partial x_3}\right|_{\mathrm{w}} = \dot{q}_{\mathrm{w}}\,. \tag{17b}$$

It is known that in turbulent flows, the profiles of $u$ and $T$ are very steep near the wall and, in addition, they undergo very strong variations. The grids previously used in TURBIT-1 and -2 [2,4,5] do not resolve this range. Therefore, it is not permitted to make linear approximations of the gradients mentioned above at the walls. In refs. [2,5], an approximation was therefore used successfully, which relies on the universal logarithmic velocity profile integrated over the mesh next to the wall. The constants contained are obviously dependent on the Grashof number in case of mixed convection as may be concluded from Wippermann [7], Back et al. [13] and Arya [14]. This dependency can also be easily indicated by the theoretical coupling of the logarithmic law of the wall with known relations on the friction coefficient; see e.g., Rotta [15]. Information about the friction factors includes at least the fact indicated by Petukhov [16] that they undergo considerable changes. For instance, the friction factor $C_f$ and the Nusselt number Nu are said to be considerably higher than in case of purely forced convection fc for data typical of the HDR downcomer (section 3), viz. $C_f/C_{ffc} = 8.92$ and $\mathrm{Nu}/\mathrm{Nu}_{fc} = 2.23$.

A reliable formulation of the law of the wall influenced by natural convection and relating to vertical channel flows can, however, not be made in the light of the present state of knowledge, since the existing criteria influencing the friction factor and the Nusselt number are contradictory [17].

Therefore, it was assumed in TURBIT-3 that the logarithmic law of the wall is not influenced by natural convection. Although this means that the quantitative evidence of the numerical results of TURBIT-3 is impaired in the case of heavily influenced mixed convection, verification of the HDR problem will show that a higher friction factor is nevertheless obtained. Moreover, in the case investigated here of a very high influence of buoyancy, the point of major turbulence energy production is displaced away from the wall into the center of flow. This means that the turbulence state obtained as well as the averaged velocity become less sensitive to inadequate wall approximations. The same problems obviously occur with molecular Prandtl numbers $\mathrm{Pr} \gtrsim 0.1$ when formulating the wall

heat flux $\dot{q}_w$ [eq. (17b)]. To avoid any additional problems in the temperature section of the computer code, the model to be simulated was considered to be adiabatic at both walls. This allows the use of a linear formulation without significant errors for the instantaneous temperature gradient at the wall. The statements concerning radial mixing are essentially influenced only in the final phase by the assumption of adiabatic walls, when the radial temperature compensation implies the disappearance of the buoyancy term. This means that a direct quantitative answer to question 1 is no longer possible. It can be answered only qualitatively.

Details of the method of calculating the SGS coefficients and of the finite difference scheme adapted so as to allow integration in space and time of the basic equations are given in ref. [2,4]. Here the main features of the method of subgrid scale modeling are discussed with particular reference to only those aspects including buoyancy effects. The momentum equation was extended in accordance with the Boussinesq approximation and the buoyancy term. This implied that for formal reasons, the extension of the subgrid scale energy equation by an additional term also became necessary. The wall approximations are not extended.

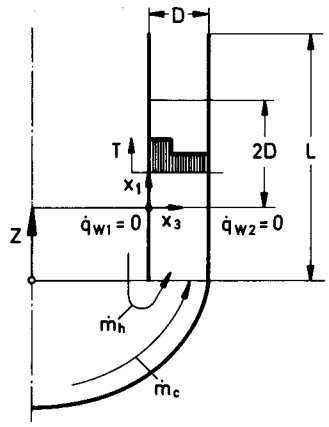


Fig. 3. Downcomer problem transferred to the computer model. The control volume of length $2D$ is temporarily at a distance $Z$ from the downcomer inlet.

## 3. Definition of initial values

In the TURBIT programs, periodical boundary conditions are applied in the main flow direction and normal to it parallel with the walls. For reasons of costs, it is hardly justified to record the total length and the whole circumference of the downcomer, the more so since this is not reasonable at all because of its periodicity, at least not in the main flow direction. Therefore, only a control volume is recorded having the length $X_1$, $X_2$ and $D$ (fig. 2) which, however, is transported thru the downcomer at the mean velocity. To describe this control volume, the proven grid K7 from ref. [2] is used. Hence, the following assumptions are made on the computational model:

– The downcomer is represented by a plane channel. The justification of this assumption can be derived from fig. 1 because of the low ratio of radii of 1.11.

– The grid possesses 16 meshes in the mean flow direction, 8 in the "circumferential direction", and 16 in the radial direction; the length of periodicity in the mean flow direction is $X_1 = 2D$ and in the $x_2$-direction ($\varphi$-direction of the pressure vessel) $X_2 = D$ (fig.2).

– In order to precalculate a limiting case, it is assumed that the two mass flows with the temperatures $T_h = 310°C$ and $T_c = 252.5°C$ enter the downcomer without mixing (fig. 3).

– The space portions of the hot and cold zones correspond to the ratio each of the two mass flows ($\hat{m}_h = 62.4$ t/h and $\hat{m}_c = 180$ t/h).

– The walls are adiabatic.

– The dimensionless numbers to be specified are predetermined in accordance with the material values for water at a pressure of 110 bar. Thus the molecular Prandtl number is Pr = 0.89.

– The Reynolds number to be specified $Re_\tau = Re_0 = 3300$ results in the normalization selected from the friction coefficient law according to Blasius. The related Reynolds number calculated with the channel width $\hat{D} = 0.15$ m and the averaged velocity is Re = 72 440.

– The Grashof number to be specified in the mean flow direction, $Gr_{01}$, is calculated by means of $\hat{T}_{w1} = \hat{T}_h$ and $\hat{T}_{w2} = \hat{T}_c$, which means by use of the zone temperatures. $Gr_{01} = -2.27 \times 10^{10} < 0$, since the vector of gravitaty $g$ in the positive $x_1$-direction is set positive. The transverse components of the buoyancy term are zero because of the vertical arrangement, implying $Gr_{02} = Gr_{03} = 0$.

To start the integration of the non-stationary 3-

dimensional equations of conservation for mass, momentum and enthalpy, the entire 3-dimensional fields for $u_i$ and $T$ must be predetermined at the time $t = 0$. Since both mass flows are directed along walls (core barrel inner face and pressure vessel bottom) when approaching the downcomer inlet, it is assumed that the velocity field during entry of the downcomer has almost fully developed. The respective initial values are derived from integration results available for the same grid. For this purpose, the averaged velocity profile is corrected according to the universal logarithmic wall laws for the Reynolds number under consideration, and the statistical properties of the velocity variations are taken over without modifications.

To obtain a conservative estimate of the mixing behaviour, the temperature field is completely decoupled statistically from the velocity field. It is assumed that the averaged temperatures are constant in the radial direction within the two zones. They are superimposed by a fluctuating part with a maximum amplitude of 1%, generated by a psuedo random number generator. This ensures the consistency of the selected initial conditions because constant profiles are associated with a radial turbulent heat flux of the order of zero, which can be obtained most conveniently in the specification by complete decoupling of the velocity and temperature fields.

To better judge the influence of buoyancy, a numerical simulation is first made in which at $Gr_{01} = 0$, influences of buoyancy are not effective. This simulation therefore treats the mixing behaviour of a passive scalar variable in purely forced convection. The rest of input data are identical with the case specified above.

## 4. Evaluation of the results of simulation

Starting from the initial values indiciated above, the system of equations underlying the method of simulation was integrated over 20 and 45 min, respectively, of CPU-time on the IBM 370/168 installed at the Karlsruhe Nuclear Research Center (Table 1). Of the non-stationary, 3-dimensional results obtained for the three velocity components, the pressure, the temperature and the subgrid-scale energy, a complete data set was stored on magnetic tape for each sixtieth time interval only. Because of the periodical boundary conditions, it is possible to evaluate these data by averaging over surfaces parallel to the wall so that the expensive ensemble averaging over several simulations with differing statistical initial fields can be avoided.

The periodical boundary conditions, on the other hand, transform the control volume into a plane channel of infinite extension. Consequently, the axial development of the flow fields cannot be considered without expensive additional transformations [2, p. 65] in a meaningful way within the control volume. Therefore, the control volume is transported here at the averaged velocity through the downcomer, and the axial development in the downcomer is concluded from the time dependent development in the control volume. Since during this process, axial gradients cannot act upon the control volume, the numerical results have to be considered as merely qualitative. Thus, all results indicated below haven been converted into the path $Z$ covered (see fig. 3) in the downcomer using the averaged velocity of the control volume and problem time. When discussing the numerical results, the averages $v$- and $j$- are omitted for the sake of simplicity. However, because of eq. (7a), all temperatures are

Table 1
Some final results of both numerical simulations. NT = number of time steps; the final values are identified by the subscript max

| Case | $Gr_{01}$ | CPU-time (min) | NT | $t_{max}$ | $Z_{max} = \int_0^{t_{max}} {}^{v}\langle u_1 \rangle \, dt$ | $\Delta T_W(Z_{max})$ | $Gr_1(Z_{max})$ |
|---|---|---|---|---|---|---|---|
| I | 0 | 19.3 | 1020 | 2.33 | 50.38 | 0.285 | 0 |
| II | $-2.27 \times 10^{10}$ | 44.3 | 2280 | 2.14 | 32.36 | $0.5 \times 10^{-3}$ | $-1.1 \times 10^{7}$ |

obviously mesh volume averaged values, and because of eq. (7b), all velocities are mesh surface averaged values. At the rms-values of the temperature fluctuations, the isotropic subgrid-scale portions according to [2, appendix 6] are added to the directly resolved large-scale portions and in case of turbulent heat fluxes the subgrid scale portions eq. (9b).

### *4.1. Decay of the temperature field in purely forced convection*

In case I, the calculated temperature field, as a passive scalar quantity, is in the parameter range under consideration essentially a function of the turbulent velocity fields only. Therefore, its maximum credibility cannot exceed those of the latter. The TURBIT computer code was previously compared extensively with experimental results for forced convection in annular gaps and plane channels [2,5,18]. In the case considered here, the numerical results of the momentum portion are therefore not validated by experimental results.

Within the prescribed computer time, the control volume covers a path of $Z_{max} \approx 50.4$ (table 1). This value agrees quite well with the length of the downcomer according to fig. 1, which is $L = 7.57$ m/0.15 m $\approx 50.5$. Consequently, the final values of this simulation can be considered as directly applicable to the outlet of the downcomer.

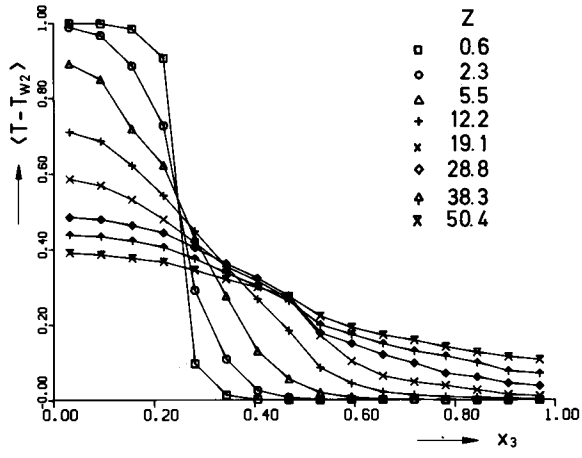


Fig. 4. Radial temperature profiles for different distances $Z$ from the entrance of the downcomer in the case of purely forced convection (case I).

For detailed evaluation the development of the temperature profile, the rms-value profile, and the radial turbulent heat flux profile have been indicated in the HDR-downcomer as general representations for selected points $Z$ in figs. 4 to 6. The partly irregular profiles can be attributed to inadequate averaging. The planes parallel to the wall obviously contain too low a mesh number to achieve reliable averaging. The temperature profile (fig. 4) first reveals a quick and subsequently a slower decay. First, at $Z = 2.3$, the nearer hot wall is reached by the mixing zone. The more distant cold wall is reached between $Z = 12$ and 19. The subsequent reduction of temperature differences takes place almost symmetric to the channel center.

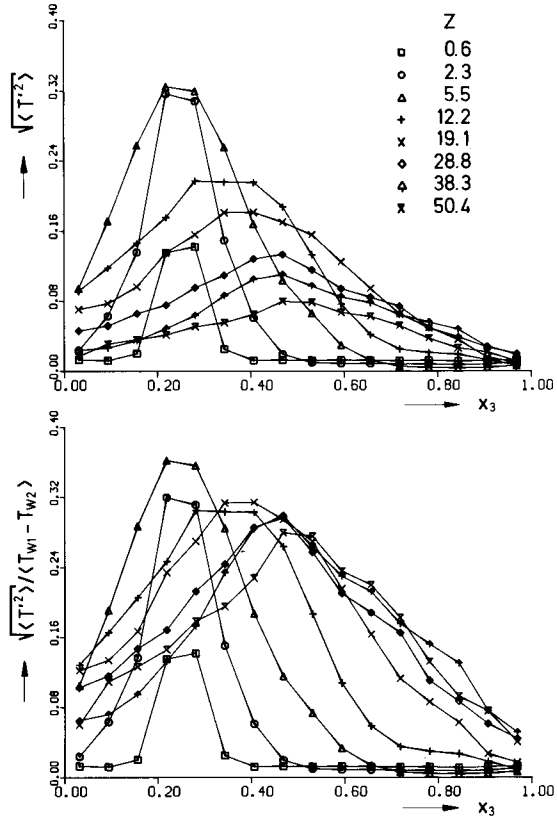


Fig. 5. Radial rms value profiles (rms – root mean square) of the temperature fluctuations in purely forced convection (case I). Normalization using the local wall temperature difference involves that the profiles in the upper half of the downcomer get nearly independent of $Z$.

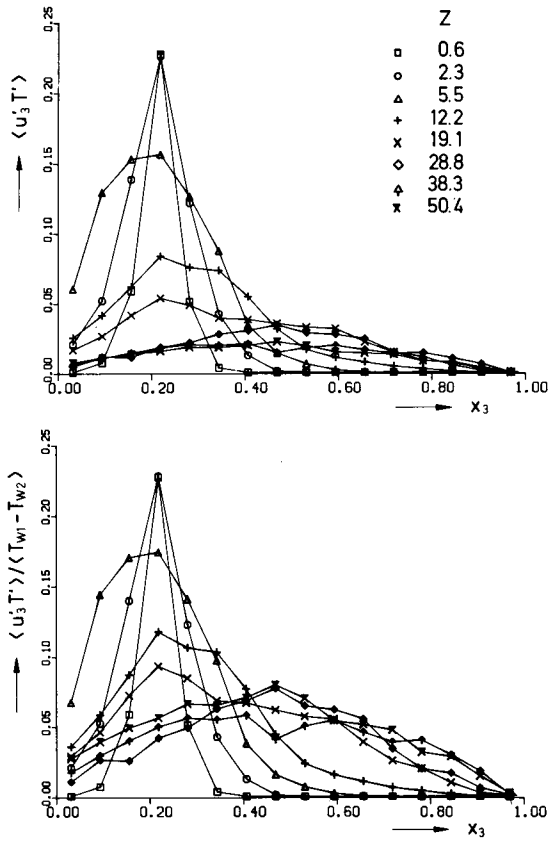


Fig. 6. Radial profiles of the radial turbulent heat flux in purely forced convection (case I). Normalization using the local wall temperature difference involves that the profiles in the upper half of the downcomer get nearly independent of $Z$.

It can be seen from figs. 5 and 6 that the quick decay at the beginning is paralleled by high temperature fluctuations and also by high turbulent heat fluxes in the positive $x_3$-direction, i.e. towards the colder zone. Both variables developed so quickly that they reached their absolute maxima as early as at $Z = 5.5$ and decrease again for a higher value of $Z$.

The conclusion might be drawn that the influence of the selection of statistically decoupled initial temperature values is low, which means that it corresponds to a maximum uncertainty in the axial coordinate of $\Delta Z \approx 5$. The respective maxima of the profiles of both variables do not occur next to the wall, as is the case for non-adibatic walls, but in the region of the maximum radial temperature gradient. If the profiles are normalized to the local wall temperature differences, both the rms-temperature value profiles and the profiles of the radial turbulent heat flux become nearly independent of $Z$ for a high value of $Z$, which means that the entrance effects of the channel have nearly vanished and an equilibrium condition has been obtained.

At the end of simulation, which means approximately at the upper end of the downcomer, there is still a wall temperature difference of 28.5% related to the initial value (table 1). This means that the compensation of temperature is far from being terminated; this likewise appears from the radial turbulent heat flux at the end of simulation, which differs markedly from zero. For case II, influenced by buoyancy, the conclusion might be drawn that the local Grashof number is insignificantly reduced by the low reduction of the local wall temperature difference only so that considerable buoyancy influences would have to be expected at the outlet of the downcomer.

### *4.2. Decay of the temperature field in case of mixed convection*

The path covered by the control volume within the given computer time is only $Z_{max} = 32.4$ in case II of the forced convection, heavily influenced by buoyancy (table 1). Despite the longer computer time by a factor of 2.3 as compared to case I, this path is

Table 2
Development of the local Grashoff number $Gr_1$, the averaged velocity $^{v}\langle u_1 \rangle$, and the ratio of friction coefficients over $Z$

| $Z$ | $-Gr_1$ | $^{v}\langle u_1 \rangle$ | $C_f/C_{ffc}$ | $C_f/C_{ffcPet}$ |
|---|---|---|---|---|
| 0.6 | $0.227 \times 10^{11}$ | 21.39 | 1.07 | 9.11 |
| 1.3 | $0.227 \times 10^{11}$ | 20.87 | 1.12 | 9.33 |
| 2.0 | $0.223 \times 10^{11}$ | 20.42 | 1.16 | 9.47 |
| 2.7 | $0.174 \times 10^{11}$ | 18.98 | 1.32 | 9.23 |
| 3.6 | $0.134 \times 10^{11}$ | 17.14 | 1.58 | 9.20 |
| 4.7 | $0.966 \times 10^{10}$ | 15.62 | 1.86 | 8.86 |
| 5.9 | $0.328 \times 10^{10}$ | 14.88 | 2.02 | 6.06 |
| 7.2 | $0.686 \times 10^{9}$ | 14.42 | 2.13 | 3.39 |
| 9.0 | $0.279 \times 10^{9}$ | 14.35 | 2.15 | 2.44 |
| 11.2 | $0.140 \times 10^{9}$ | 14.32 | 2.16 | 1.93 |
| 15.6 | $0.643 \times 10^{8}$ | 14.40 | 2.14 | 1.53 |
| 19.8 | $0.391 \times 10^{8}$ | 14.55 | 2.10 | 1.35 |
| 26.1 | $0.216 \times 10^{8}$ | 14.85 | 2.03 | 1.20 |
| 32.4 | $0.114 \times 10^{8}$ | 15.16 | 1.96 | 1.11 |

nevertheless smaller by a factor of 1.6. A main reason is the occurrence of locally, very high velocities which, via the time interval automatism according to Schumann [19], strongly reduce the reliable time interval for the explicit integration technique. Although the path covered is shorter than the length $L$ of the downcomer, it nevertheless allows conclusions to be drawn for the HDR downcomer problem with a sufficient accuracy.

The velocity ${}^{v}\langle u_1 \rangle$ averaged over the control volume is shown in table 2, as an integral variable for the velocity field. The averaged velocity and hence the Reynolds number actually obtained are not constant since in TURBIT-3, normalization variables are used which are defined as being constant. The averaged velocity decreases quickly, remains constant until $Z = 5$ over a large range, and subsequently rises slowly again at the end of simulation. This particular feature of simulation also allows to draw but qualitative conclusions for HDR since the changes accordingly reduce the actual Reynolds number by 30%.

The comparison of the increased friction factor with respect to forced convection with the Petukhov criterion [16] shows that, nevertheless, the numerical results can be compared quantitatively (table 2). The ratio $C_f/C_{ffc}$ of the friction coefficients after a short entrance length attains its maximum value of 2.16 at $Z = 9$–$11$. This value agrees rather well with the value obtained for fully developed flows according to the Petukhov criterion, if one uses the respective local dimensionless numbers. Subsequently, the Petukhov result remains under the numerical one and, accordingly, the averaged velocity rises again. This confirms that in the case studied, neglecting the influences from buoyancy on the formulation of the wall approximation actually has no remarkable practical influence on the numerical results.

The development of the numerically simulated velocity and temperature profiles appears from the general representations of figs. 7 and 8. Fig. 7 gives an impression of the initial phase of simulation. The fluid is considerably accelerated at the hot wall and substantially decelerated at the cold wall. At $Z = 1.3$ reflow occurs over more than 60% of the channel section. Although the spatial extension of reflow is reduced at a higher value of $Z$ by increase of temperature in the previously cold region of the mixing zone, the maximum reflow velocity continues to rise. Already

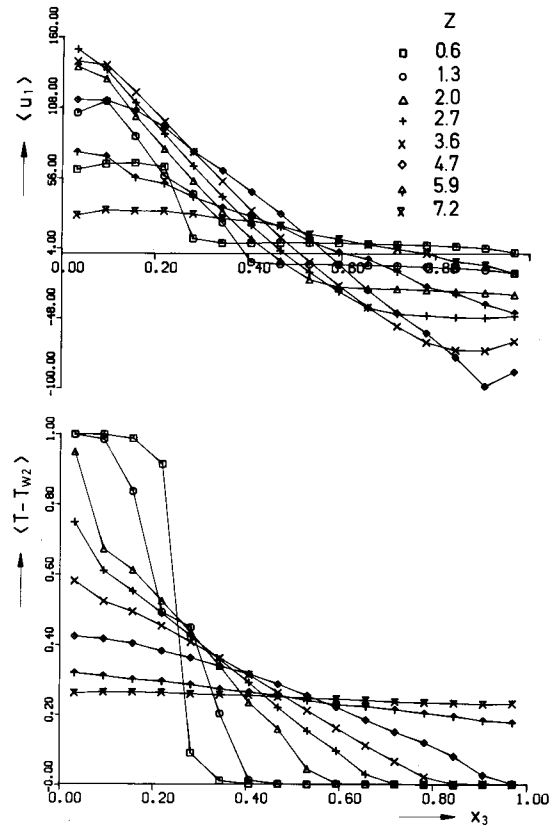


Fig. 7 Radial velocity and temperature profile in the entrance region of the downcomer up to $Z = 7.2$ under condition of mixed convection (case II). The maximum velocity is attained at about $Z = 2.7$, the minimum velocity at $Z = 4.7$.

at $Z = 2.7$ the positive velocity in the hot zone reaches its absolute maximum value of approximately 7 times the averaged initial velocity since the temperature is reduced quickly in this zone. For greater values of $Z$ this maximum value initially decreases at a low rate only.

The absolute minimum of velocity, i.e., the absolute maximum value of reflow velocity, reaches 4.5 times the averaged initial velocity at $Z = 4.7$. At this point, the cold wall is reached by the mixing zone in the temperature field. This means that the pressure difference caused by buoyancy

$$\Delta p_{nc}(x_3) = \frac{Gr_{01}}{Re_0^2}({}^{v}\langle T \rangle - \langle T(x_3) \rangle) \qquad (18)$$

is reduced also in the cold zone by progressing flatten-

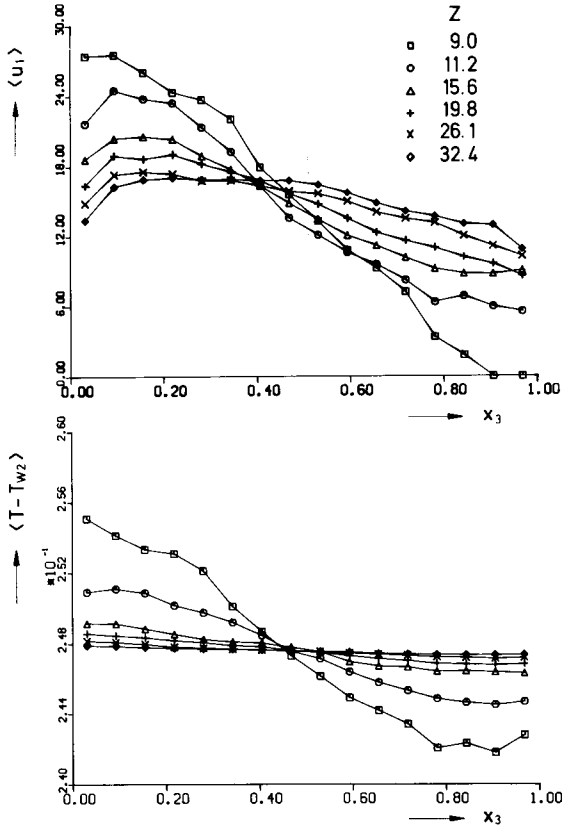


Fig. 8. Radial velocity and temperature profiles for $Z \geq 9$ under condition of mixed convection (case II). At $Z > 9$ local reflow does no longer occur.

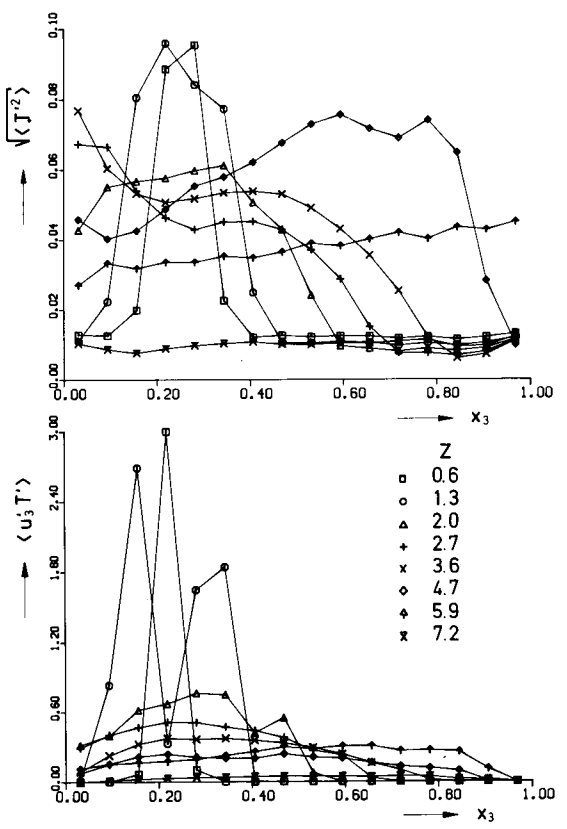


Fig. 9. Radial profiles of the rms values of the temperature fluctuations and the radial turbulent heat flux in the entrance region of the downcomer up to $Z = 7.2$ under condition of mixed convection (case II).

ing of the temperature profile. Subsequently, these profiles undergo quick changes. At $Z = 7.2$, the temperature profile seems to be largely linear and constant. Here, the temperature difference between the two walls amounts to only about 9% of the initial value. The positive and negative extreme values of velocity are reduced accordingly. It gets obvious that this simulation provides a quicker decay of the temperature field than that for purely forced convection (section 4.1).

The end of local reflow in the cold zone can be found at roughly $Z = 9$ (fig. 8). The related temperature profile makes visible differences from the final result or the volume averaged temperature ${}^{v}\langle T \rangle = 0.248$ with a modified imaging scale only because the wall temperature difference has decreased to about 1% of the initial value. The suppression of reflow already at this point is surprising since the local net difference of driving pressure near the cold wall is still negative.

$$\left[ -\left\langle \frac{\partial p}{\partial x_1} \right\rangle + \Delta p_{nc} \right]_{Z=9, x_3=0.03} \approx -8$$

Obviously, this introduction of local axial negative momentum is overcompensated by the turbulent momentum which is transverse relative to the mean flow direction. The net difference of the driving pressure is positive in the entire channel for $Z > 17.6$ only.

At the end of simulation for $Z = 32.4$, the velocity profile is nearly symmetric again because the compensated temperature field exerts practically no more influence on the net difference of the driving pressure (fig. 8).

According to table 1, the wall temperature difference decreases to only 0.5‰ of the initial value. The related local Grashof number has reduced accordingly by more than 3 orders of magnitude.

It can be explained by the profiles of the temperature fluctuations and the radial turbulent heat flux how the quick reduction of the temperature differences is brought about. Fig. 9 shows that the quick decay of the temperature field is related to high temperature fluctuations for small values of $Z$ and also to high radial turbulent heat fluxes in the positive $x_3$-direction, i.e., towards the colder zone. The respective maxima of the profiles of both variables neither occur near the wall as is the case during forced convection in channels having non-adiabatic walls, but rather as in case I and, as indicated by Carr et al. [20] and Brown and Gauvin [21], at some distance from the wall and obviously in agreement with the results by Kotsovinos [22], near the maxima of the radial temperature gradient and the radial velocity variations respectively.

The quantitative comparison with the case of forced convection makes evident that the radial heat flux developing here is greater by approximately the factor 3–5 (fig. 6) and the rms-values of temperature fluctuations are accordingly lower (fig. 5). The effects on the temperature field can be derived qualitatively: As observed in experiments on plane jets, performed by Kotsovinos [22], the buoyancy, contrary to the simulation without buoyancy effects, also in this case leads to doubling of the velocity fluctuations and thus tends to increase the radial turbulent heat flux. The latter results in a faster reduction of radial temperature differences. Since the temperature fluctuations can be generated only in zones characterized by temperature differences and it is known that they require much longer distances for generation than the temperature profile itself, smaller rms temperature values are obtained in the temperature field decaying at a faster rate.

The profiles of fig. 9 normalized by the local wall temperature differences are represented in fig. 10. Within the range represented up to $Z = 7.2$, the rms temperature value and the radial heat flux increase. Results independent of $Z$ have not yet been obtained. Only for $Z > 7.2$, approximately constant results are obtained at the rms value, and in the turbulent heat flux over the simulated transport length not at all (fig. 11). The cause lies in the transition of flow

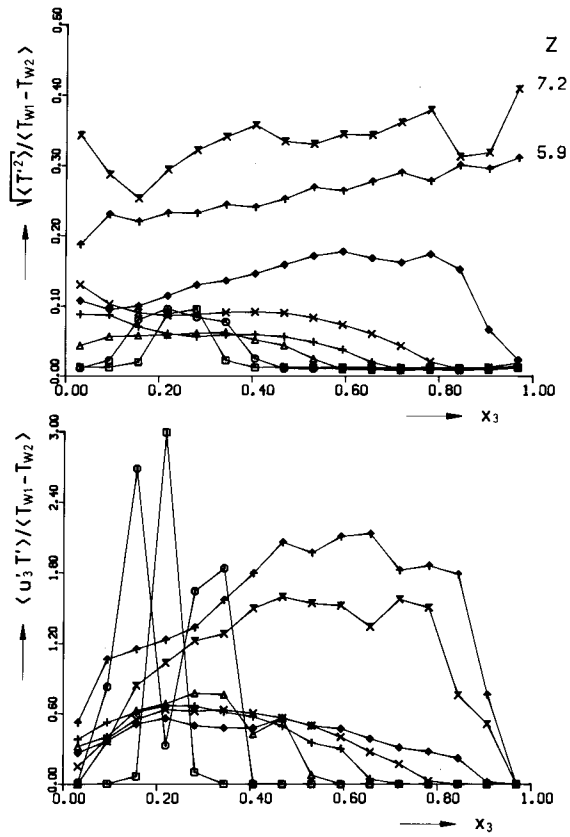


Fig. 10. Profiles of the rms values of the temperature fluctuations normalized by the local wall temperature differences and profiles of the radial turbulent heat flux up to $Z = 7.2$ (case II). Legend similar to fig. 9.

strongly influenced by buoyancy at the beginning into purely forced convection towards the end of simulation: The normalized rms temperature values have roughly the same size in the case of forced convection (fig. 5) and mixed convection (fig. 11) except for the shapes of profiles which result from the S-shaped and linear temperature profiles, respectively. By contrast, the normalized radial heat flux is greater by nearly one order of magnitude because of the faster compensation of temperatures (figs. 10 and 11) as compared with forced convection (fig. 6). This difference is reduced with decreasing influence of buoyancy so that towards the end of simulation at $Z = 32.4$ a heat flux profile develops which is comparable with that of forced convection. This means that the results found here are inherently consistent and compatible

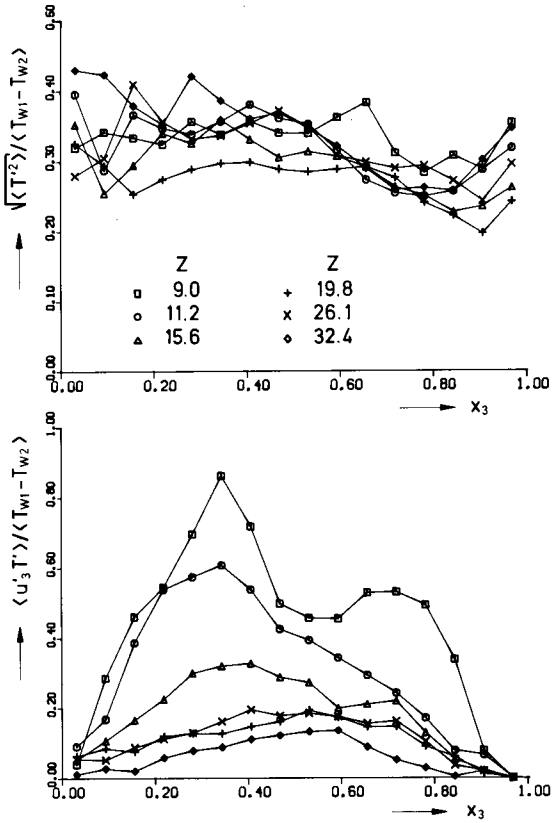


Fig. 11. Profiles of the rms values of the temperature fluctuations normalized by the local wall temperature differences and profiles of the radial turbulent heat flux for $Z > 9$ (case II).

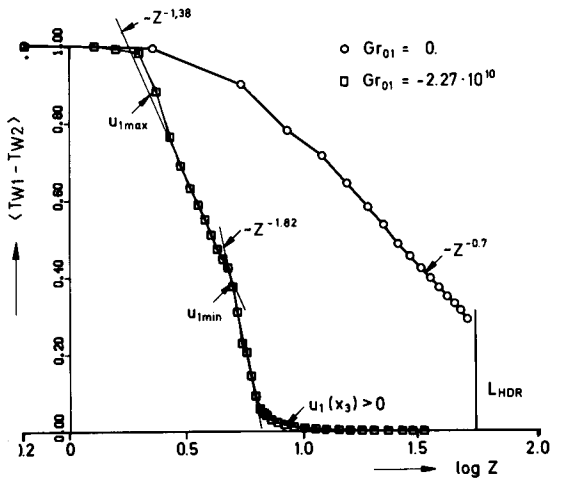


Fig. 12. Decrease of difference of the wall temperatures $\Delta T_W$ over the logarithm of the axial length $Z$.

with the results given in section 4.1.

A direct quantitative verification of these results is not possible because comparable experiments are missing. It results from the experiments with vertical plane buoyant jets performed by Kotsovinos [22], who has also measured a relative rms temperature value of 40% and from the comparison of friction factors that these results are not completely useless. This finding is as well as confirmed by the results by Carr et al. [20] and Brown and Gauvin [21] which are applicable to non-adiabatic vertical channels where rms values had been found for mixed convection which were higher than the known 10–20% values of purely forced convection.

The major results to be obtained of simulating mixed convection are that in this case a much faster reduction of the wall temperature difference takes place as compared with purely forced convection. Moreover, the apprehended development of a hot self-sustaining chimney extending over the entire height of the downcomer did not occur. The reflow at the inlet is eliminated by an intensified turbulent transverse exchange for higher values of $Z$. Thus, these calculations confirm the experience that reflow develops only over the entire channel length in case of opposing pressure and buoyancy forces [8,16], which means in case of heated downard flow or cooled upward flow.

### *4.3. Decay laws for both cases*

The development of the wall temperature difference dependent on the development length has been plotted in fig. 12 for both cases on a semi-logarithmic scale. Similar to all decay processes, an exponential dependency is found also here over large ranges. In case I, the wall temperature difference follows a $Z^{-0.7}$ law. Experimental results which would be directly comparable are not available so that the behaviour of round and plane jets again or even isotropic grid turbulence must be referred to. Thus, Warhaft and Lumley [23] have found downstream of a heated grid decay laws for the rms temperature values, which correspond to $Z^{-m}$, with the exponent $m$ from 0.87 to 3.1. The value found here which, on account of fig. 5, for great values of $Z$ applies both to the rms value and to $\Delta T_W$,

is lower since inhomogeneous channel flow continuously produces new temperature fluctuations implying a slower rate of decay. For a plane jet, Chen and Rodi [24] indicate an exponent of 0.5 and for a round jet an exponent of 1.0. For the turbulent boundary layer with slot injection, which is still best comparable in a direct way, in his review paper Goldstein [25] indicates an exponent of 0.8 for the adiabatic wall effectiveness which is proportional to the wall temperature. Thus, the decay law evaluated from numerical simulation is compatible with the literature references cited above.

As to the plot for case II, four zones can be clearly distinguished: The entrance zone, two successive zones with exponential decrease, and the asymptotic decay range with $\Delta T_w \to 0$. The latter is not attained in case of simulation without natural convection at the upper end of the downcomer for $Z = L = 50.5$, since there the temperature field decays at a much slower rate.

As in case I the entrance zone is characterized by a nearly constant value of $\Delta T_w$. It ends at $Z \approx 2$. It can be concluded from the short entrance zone that the prescription of initial temperature values completely decoupled from the initial values of velocity also in case II do not exert a remarkable influence on the mixing behaviour. The minor influence of displacement by $\Delta Z = 2$ toward $\Delta T_w$ does not alter the statement that at the end of simulation influences by natural convection can be neglected.

The first exponential zone is limited by $2 < Z < 5$. Here, the wall temperature difference follows quite well a $Z^{-1.38}$ law. The end of this zone coincides with the point where the mixing zone reaches the right cold wall according to section 4.2, fig. 7, which means that it coincides also with the place where the maximum reflow velocity is established. Consequently, the wall temperature $T_{w2}$ is constant up to here. Therefore, this range can be compared best with thermal buoyant jets. The dependency found agrees well with the experience by Liburdy and Faeth [26] who state that thermal wall jets in a quiescent medium show a somewhat faster decrease than $Z^{-1}$. Moreover, the dependency found lies again between the $Z^{-1}$ law by Chen and Rodi [24] for plane buoyant and the $Z^{-5/3}$ law by Seban and Behnia [10] and Chen and Rodi [24] for round buoyant jets.

The addition "quiescent medium" is not to be considered as an other restriction of the comparison since the hot zone in the initial phase is practically governed by the buoyancy term $\Delta p_{nc}$: at the beginning it reads $\Delta p_{nc}(t = 0) = 1564 >> 2$ and hence, it is much greater than the pressure gradient imposed. Moreover, the velocity and the heat flux in this zone are greater by a multiple as compared with purely forced convection.

The second exponential zone is limited by the condition $5 < Z < 6.4$. Here a $Z^{-1.82}$ law roughly applies. The decrease of $\Delta T_w$ is obviously steeper than in the first exponential zone since here both wall temperatures are changed by turbulent mixing. Compared with the $Z^{-0.7}$ reduction for case I, we found here much steeper exponential reductions of $\Delta T_w$. At the end of this region $\Delta T_w$ has been reduced to already 6% of the initial value.

The asymptotic transition of $\Delta T_w$ towards zero can be evaluated less from fig. 12 than from table 2. The order of magnitude of the local Grashof number and, hence, also the wall temperature difference are further reduced quite markedly here. At the end of simulation $5 \times 10^{-4}$ of the initial wall temperature difference remains. The related local Grashof number has decreased accordingly to $1 \times 10^7$. Consequently, in this zone the buoyancy term is smaller than the imposed pressure gradient.

Hence, with respect to the HDR problem it can be shown with adequate certainty that the strong influences of buoyancy act stabilizing when entering the downcomer in the sense that they decay at a relatively fast rate so that at the upper end of the downcomer no more effects can be found and the two entering fluid mass flows are adequately mixed.

## 5. Conclusions for the problem of enthalpy stratification in the HDR

To discuss the influence exerted by natural convection effects in the HDR-downcomer it is significant for the setting of reactor typical initial conditions for blowdown tests to know how stable radial temperature discontinuities are in the downcomer and how fast they are reduced in case of flow passage through the downcomer. This problem for which comparable experimental results have not been known previously, is studied by means of the numerical direct simulation technique realized in the TURBIT-3 computer code.

To consider consistently the influences by buoy-

ancy in the computer code both the complete Navier-Stokes equations were extended by the buoyancy term in form of the Boussinesq approximation and the energy equation for subgrid scale structures used in the subgrid scale model was extended by the related production term. When formulating the wall conditions some problems remain unsolved according to the present state of knowledge regarding mixed convection. However, the results allow the conclusion to be drawn that in the case under consideration the extensions introduced, especially as regards the energy equation, are of greater importance than an exact formulation of the wall conditions. By this and due to some problems such as the application of periodical boundary conditions and the special type of normalization, the numerical results obtained can be transferred only qualitively to the entrance problem of the downcomer.

As a limiting approximation for the HDR-problem the decay of a jump in the radial temperature profile was studied for an adiabatic channel, as may occur by insufficient mixing at the inlet to the downcomer. Influences by natural convection had not been considered initially. It appeared that in purely forced convection serious mixing of both temperature zones is not expected. The difference of wall temperatures remaining at the upper end still amounts to about 25% of that at the lower end. After a short entrance length the wall temperature difference follows an exponential decay law.

By contrast, a second simulation in which the influences of buoyancy are taken into account, provides much quicker mixing. The radial velocity profiles determined are characterized in the entrance zone by high accelerations in the hot zone and decelerations in the cold zone. Thus, within the first nine channel widths considerable reflow occurs in the cold zone which, actually, would lead to intensive mixing at the HDR inlet of the downcomer. Downstream of the area of reflow the influence of the buoyancy term disappears very quickly so that even towards the end of simulation conditions of quasi-forced convection are encountered. Thus, in this simulation, the formation of continuous hot "chimneys" was not observed and is certainly not to be expected in the downcomer of the HDR, provided that the radial heat losses from the pressure vessel are negligible as compared with the rest of heat fluxes.

The evaluation of the temperature difference being established between the hot internal wall and the cold external wall of the downcomer leads to a much quicker reduction over the axial length than in case of simulation without influences of buoyancy. The wall temperature difference follows two exponential decay laws: it follows a $Z^{-1.38}$-law in the entrance zone and, subsequently, after the mixing zone has spread over the whole channel in the radial direction, it follows a $Z^{-1.82}$-law. In the following asymptotic transition towards zero the wall temperature difference falls below the 1 per thousand limit after having passed half the length of the downcomer. The influence of buoyancy is of minor importance for subsequent development.

By the examples of the radial turbulent heat fluxes evaluated from both simulations it was shown how the influence of buoyancy leads to the quicker mixing of both temperature zones through an intensified production of turbulence in the entrance zone. The results of temperature field statistics were verifiable at least in some points despite the lack of adequate experimental information. Besides, they are consistent with the rest of results and also compatible with those of the simulation without buoyancy. They allow the conclusion to be drawn that in the not ideal adiabatic reality of the HDR downcomer even slightly faster mixing of the cold and hot zones can be anticipated. Hence, in the available results of simulations, no phenomenon was found which would require a change in testing aimed at the adjustment of enthalpy stratification at the HDR reactor. After closing this theoretical investigation, measurements of the temperature field have been made in the HDR reactor which are in accordance with this conclusion [27].

This calculation of an engineering like problem using the TURBIT–3 computer code shows that the direct numerical simulation technique together with a subgrid scale model of the single transport equation type is a very helpful tool not only in basic research. Compared with the statistical turbulence models currently used, the expenditure in terms of computer time with this method is comparable since expensive test calculations due to "the battle of the constants" can be largely avoided. The model assumptions exert only a weak influence on the results. They possess a larger range of validity. Moreover, direct numerical

simulation when using the classification by Saffman [28], constitutes the only method which must not be used only as a "postdictive" but also as a "predictive" one.

## Nomenclature

*Operator notation for any quantity Y*

| | |
|---|---|
| $Y$ | = any dimensionless quantity |
| $\hat{Y}$ | = any dimensional quantity |
| ${}^{v}\overline{Y}$ | = volume mean value, eq. (7a) |
| ${}^{j}\overline{Y}$ | = surface mean value for the surface ${}^{j}F$ with the normal in the $x_j$-direction eq. (7b) |
| $\langle Y \rangle$ | = time or ensemble mean value |
| ${}^{v}\langle Y \rangle$ | = mean value taken over the flow volume recorded |
| $Y'$ | = deviation from a mean value |
| ${}^{v}\overline{Y}'$ | = volume mean value of the subgrid scale structure |
| $\delta_j$ | = finite difference operator in the $x_j$-direction, eq. (7b) |
| $\delta_{ij}$ | = Kronecker delta |

*Latin symbols*

| | |
|---|---|
| $a$ | = thermal diffusivity |
| $C_j$ | = subgrid scale coefficients |
| $C_f$ | = friction factor |
| $D$ | = channel width |
| $E$ | = kinetic energy |
| ${}^{j}F$ | = surface area of a grid surface with the normal in the $x_j$-direction |
| $g$ | = acceleration due to gravity |
| Gr | = Grashof number, eqs. (2) and (5) |
| $h$ | = characteristic width of grid cell |
| $l$ | = mixing length |
| $L$ | = length of downcomer (fig. 3) |
| $\dot{m}$ | = mass flow rate |
| Min$(a, b)$ | = minimum between $a$ and $b$ [Min$(a, b)$ = $a$ for $a < b$ and vice versa] |
| $p$ | = pressure |
| Pr | = molecular Prandtl number, eq. (2) |
| $\dot{q}$ | = heat flux |
| Re | = Reynolds number, eqs. (2) and (5) |
| $t$ | = time |
| $T$ | = temperature |
| $u$ | = velocity, according to fig. 2 |
| $x_j$ | = local coordinate in the computer model (figs. 2 and 3) |
| $\Delta x_j$ | = width of grid cell in the $x_j$-direction |
| $X_j$ | = periodicity length in the $x_j$-direction (fig. 2) |
| $Z$ | = axial coordinate in the downcomer (fig. 3) |

*Greek symbols*

| | |
|---|---|
| $\beta$ | = volume expansion coefficient $\hat{\beta} = -1/\hat{\rho}(\partial\hat{\rho}/\partial\hat{T})$ |
| $\epsilon$ | = dissipation |
| $\mu$ | = turbulent SGS viscosity for momentum |
| $\nu$ | = kinematic viscosity |
| $\rho$ | = density |
| $\tau$ | = shear stress |

*Subscripts*

| | |
|---|---|
| c | = cold |
| fc | = forced convection |
| h | = hot |
| HDR | = Heiss-Dampf-Reaktor (superheating steam reactor) |
| i, j | = subscript for direction (fig. 2) |
| nc | = natural convection |
| t | = turbulent |
| T | = temperature part of equations |
| w 1, 2 | = wall values at $x_3 = 0, D$ |
| $\tau$ | = related to wall shear stress (velocity), eq. (3) |
| 0 | = normalized variable at time $t = 0$ |

## Acknowledgements

The author thanks Dr. W. Rodi, Sonderforschungsbereich 80, Universität Karlsruhe, for numerous suggestions and some literature references. Further thanks are due to Dr. M. Bottoni and Mr. Mösinger who read the paper carefully.

## References

[1] R. Krieg, E.G. Schlechtendahl and K.H. Scholl, Nucl. Eng. Des. 43 (1977) 419.

[2] G. Grötzbach, Direkte numerische Simulation turbulenter Geschwindigkeits-, Druck- und Temperaturfelder bei Kanalströmungen, KfK 2426 (1977).
[3] J.W. Deardorff, J. Fluid Mech. 41 (1970) 453.
[4] U. Schumann, J. Comput. Phys. 18 (1975) 376.
[5] G. Grötzbach, in: Lecture Notes in Physics, Vol. 76 (Springer-Verlag, Berlin, 1978) p. 308.
[6] J.S. Turner, Buoyancy effects in fluids (Cambridge Univ. Press, Cambridge, 1973).
[7] F. Wippermann, The planetary boundary layer of the atmosphere. (Deutscher Wetterdienst, Offenbach, 1973).
[8] J. Khosla, T.W. Hoffmann and K.G. Pollock, in: Proc. 5th Int. Conf. Heat Transfer, Tokyo (1974) Paper NC 4.4.
[9] A.T. Wassel and I. Catton, Int. J. Heat Mass. Transfer 20 (1977) 383.
[10] R.A. Seban and M.M. Behnia, Int. J. Heat Mass. Transfer 19 (1976) 1197.
[11] J.W. Deardorff, in: Proc. Workshop Micrometeorology, Ed. D.A. Haugen (American Meteorological Society, 1973) p. 271.
[12] G. Lörcher, Laser-Doppler-Messungen von Energiedichtespektren in turbulenter Kanalströmung, KfK 2448 (1977).
[13] L.H. Back, R.F. Cuffel and P.F. Masaier, Int. J. Heat Mass Transfer 13 (1970) 1029.
[14] S.P.S. Arya, J. Fluid Mech. 68 (1975) 321.
[15] J.C. Rotta, Turbulente Strömungen (B.G. Teubner, Stuttgart, 1972).
[16] B.S. Petukhov, in: Proc. Int. Seminar Turbulent Buoyant Convection, Dubrovnik, Aug. 30–Sept. 4, 1976, Eds. D.B. Spalding and N. Afgan (Hermisphere, 1977) p. 701.
[17] G. Grötzbach, Numerische Untersuchung der Quervermischung bei auftriebsbeeinflusster turbulenter Konvektion in einem vertikalen Kanal, KfK 2648 (1978).
[18] G. Grötzbach, and U. Schumann, in: Symp. Turbulent Shear flows, Pennsylvania State University, April 18–20, 1977, Eds. F. Durst, F.W. Schmidt, J.H. Whitelaw and B.E. Launder (Springer-Verlag, Berlin, 1979), p. 370.
[19] U. Schumann, J. Comput. Phys. 18 (1975) 465.
[20] A.D. Carr, M.A. Connor and H.O. Buhr, J. Heat Transfer 95 (1973) 445.
[21] C.K. Brown and W.H. Gauvin, Chem. Eng. Sci. 21 (1966) 961.
[22] N.E. Kotsovinos, J. Fluid Mech. 81 (1977) 45.
[23] Z. Warhaft and J.L. Lumley, in: Lecture Notes in Physics, Vol. 76 (Springer-Verlag, Berlin, 1978) p. 113.
[24] C.-J. Chen and W. Rodi, in: Proc. 6th Int Conf. Heat Transfer, Toronto, Aug. 7–11, 1978, Vol. 1, p. 97.
[25] R.J. Goldstein, in: Advances in Heat Transfer, Vol. 7 (Academic Press, New York, 1971) p. 321.
[26] J.A. Liburdy and G.M. Faeth, in: Proc. ASME-Winter Anual Meeting, Atlanta, Georgia, Nov. 27–Dec. 2, 1977, ASME-Paper 77-WA/HT-30.
[27] E. Erb, G. Grötzbach, F. Katz, R. Krieg, A. Ludwig, H. Mösinger, W. Olbrich, P. Philipp, H. Schnauder and U. Schumann, Projekt Nukleare Sicherheit, Halbjahresbericht 1978/1 (KfK 2700, 1978) p. 4100-1.
[28] P.G. Saffman, in: Lecture Notes in Physics, Vol. 76 (Springer-Verlag, Berlin, 1978) p. 273.